AGU PUBLICATIONS

Geophysical Research Letters

Key Points:
- A novel record of 90 icebergs in Sermilik Fjord indicates that icebergs are subject to strongly sheared flows over the range of their draft
- Icebergs are able to move fastest when their drafts are around the depth of the interface between the upper and lower fjord layers
- Ocean shear has a leading order impact on iceberg velocity and melt rate and should be incorporated into models of iceberg motion and melt

Supporting Information:
- Supporting Information S1

Correspondence to:
A. FitzMaurice,
apf@princeton.edu

Effect of a sheared flow on iceberg motion and melting

A. FitzMaurice[1], F. Straneo[2], C. Cenedese[2], and M. Andres[2]

[1]Program in Atmospheric and Oceanic Sciences, Princeton University, Princeton, New Jersey, USA, [2]Woods Hole Oceanographic Institution, Woods Hole, Massachusetts, USA

Abstract Icebergs account for approximately half the freshwater flux into the ocean from the Greenland and Antarctic ice sheets and play a major role in the distribution of meltwater into the ocean. Global climate models distribute this freshwater by parameterizing iceberg motion and melt, but these parameterizations are presently informed by limited observations. Here we present a record of speed and draft for 90 icebergs from Sermilik Fjord, southeastern Greenland, collected in conjunction with wind and ocean velocity data over an 8 month period. It is shown that icebergs subject to strongly sheared flows predominantly move with the vertical average of the ocean currents. If, as typical in iceberg parameterizations, only the surface ocean velocity is taken into account, iceberg speed and basal melt may have errors in excess of 60%. These results emphasize the need for parameterizations to consider ocean properties over the entire iceberg draft.

1. Introduction

The mass flux to the ocean from the Greenland and Antarctic ice sheets comprises surface melt leaving the ice sheets as runoff and subglacial discharge, subsurface melt where the ice meets the ocean, and the calving of icebergs directly into the ocean. Of these, iceberg calving is thought to contribute approximately half the mass loss in both Greenland and Antarctica, representing a mass flux of roughly 500 km^3 yr^{-1} from Greenland [*Enderlin and Howat*, 2014; *Rignot et al.*, 2008] and 1300 km^3 yr^{-1} from Antarctica [*Depoorter et al.*, 2013].

Given the increase in mass loss from both poles in recent decades [*Bamber and Aspinall*, 2013; *Rignot et al.*, 2011], understanding where and how this meltwater enters the ocean is important to the ocean circulation, particularly in the North Atlantic where localized surface-concentrated freshwater fluxes may result in the capping of deep convection sites, with potential implications for the Atlantic Meridional Overturning Circulation [e.g., *Srokosz et al.*, 2012; *Zickfeld et al.*, 2007]. Accurate modeling of iceberg motion and melt is necessary to describe this meltwater flux and hence capture the ocean's response to increased mass flux from Greenland and Antarctica. In addition to these physical considerations, from a biological perspective icebergs are important in supplying nutrients to the ocean, and enhanced biological activity has been observed in their melt plumes [*Duprat et al.*, 2016]. To predict when and where such blooms may occur, and how their frequency and intensity may change in the future, we must first understand the underlying dynamics and thermodynamics of iceberg motion and melting.

Despite icebergs' potential importance in the climate system, little has been done to validate parameterizations of their motion and melting due to intrinsic observational difficulties. Here we investigate iceberg dynamics using an 8 month draft and speed record comprising 90 icebergs from Sermilik Fjord, southeast Greenland, following the methodology of *Andres et al.* [2015]. The large number of icebergs sampled in this study, in conjunction with local ocean current and wind data, provides an unprecedented data set with which to evaluate assumptions frequently made in modeling of iceberg dynamics and melting. The standard parameterizations used to model iceberg motion and melt in global climate models are summarized in section 2, the unique data set analyzed in this study is described in section 3, and section 4 introduces the model used to supplement these data. Results and their implications for the representation of icebergs in climate models are presented in section 5, and conclusions are drawn in section 6.

2. Background
2.1. Modeling of Iceberg Motion

In climate models, the canonical equation used to describe iceberg motion is that of *Bigg et al.* [1997] and *Gladstone et al.* [2001] (building on earlier work by *Smith* [1993] and *Mountain* [1980]), in which icebergs

are forced by a combination of surface currents and winds, sea ice and wave stresses, and surface pressure gradients. This leads to a momentum equation

$$M\frac{d\vec{u}}{dt} = -M\vec{f} \times \vec{u} + \vec{\tau}_a + \vec{\tau}_o + \vec{\tau}_i + \vec{F}_w + \vec{F}_p,$$ (1)

as in *Martin and Adcroft* [2010], for an iceberg of velocity $\vec{u}$ and mass M. Here $\vec{f}$ is the Coriolis parameter; $\vec{\tau}_a$, $\vec{\tau}_o$, and $\vec{\tau}_i$ denote air, ocean, and ice stresses, respectively; and the wave and pressure gradient forcings are $\vec{F}_w$ and $\vec{F}_p$, respectively.

In a fjord environment, it is reasonable to simplify the above full open ocean model and assume that the motion of the icebergs in our record is predominantly governed by the air and ocean forcings alone. The assumptions are fully discussed in the supporting information, and we further consider their validity when assessing our model at the end of section 4.

2.2. Modeling of Iceberg Melt

Icebergs deteriorate through surface melting from solar radiation, subsurface melting from buoyant vertical convection and forced convection, wave erosion at their margins, and calving of smaller components [*El-Tahan et al.*, 1987; *Savage*, 2001]. Surface melt is negligible compared to subsurface melt, and calving of overhanging slabs is likewise believed small [*Savage*, 2001; *Bigg*, 2016]. Thus, to model disintegration of icebergs, bottom melt M_b, subsurface side melt M_s, and wave erosion M_e are the dominant processes that must be parameterized [*Gladstone et al.*, 2001; *Martin and Adcroft*, 2010; *Bigg*, 2016]. For reference, typical maximum parameterized values for basal melt, side melt, and wave erosion rates in the open ocean are $1 \, \mathrm{m \, d^{-1}}$, $0.2 \, \mathrm{m \, d^{-1}}$, and $0.5-1 \, \mathrm{m \, d^{-1}}$, respectively [*Bigg*, 2016].

Typical parameterizations of bottom melt [e.g., *Bigg et al.*, 1997; *Savage*, 2001; *Martin and Adcroft*, 2010; *Marsh et al.*, 2015] are based on studies of forced convection past a body [*Weeks and Campbell*, 1973; *El-Tahan et al.*, 1987], with the ambient velocity of the flow past the iceberg keel taken as the surface current speed. With this parameterization, in units of $\mathrm{m \, d^{-1}}$,

$$M_b = 0.58 \, |\vec{u} - \vec{u}_o|^{0.8} \frac{T_o - T}{L^{0.2}},$$ (2)

where T_o is surface ocean temperature, T is ice temperature (assumed constant at $-4°C$), and L is iceberg length in the direction of the flow. As in equation (1), $\vec{u}$ is iceberg velocity, and now $\vec{u}_o$ is surface ocean velocity. For subsurface side melt, the parameterization is even more idealized than for basal melt. Explicitly, an empirically deduced flow-independent melt rate simply a function of the sea surface temperature is generally assumed [*Neshyba and Josberger*, 1980].

In what follows, we consider the validity of the above melt parameterizations for Sermilik Fjord icebergs. By comparing our 8 month iceberg record to concurrent ocean current speed measurements, we examine the interplay between ocean currents and iceberg dynamics and melting, quantifying potential errors accrued by the parameterizations.

3. Data

3.1. Iceberg Record

The iceberg record considered in this study was obtained from a pressure sensor-equipped inverted echo sounder (PIES) deployed in Sermilik Fjord in southeast Greenland between November 2011 and June 2012 (location shown in Figure 1). The sensor sat in the center of the fjord at a depth of approximately 860 m, emitting four 12 kHz ping bursts every 10 min. The pings bounce off strong reflectors, and the PIES recorded the time until the first reflection from each ping arrived back at the instrument. Generally, the first strong reflector encountered is the air-sea interface, but if an iceberg passes the instrument, the first reflection may come from this. Consequently, iceberg transits leave distinctive parabolic signatures in the record of early pings from the PIES as they gradually move across the sensor's field of view, as shown in Figure 1 (right). From these parabolas' curvature and minima we can estimate the iceberg's speed and draft. The data collection methodology and theory underlying iceberg speed and depth estimation are described in detail in *Andres et al.* [2015].

In our study iceberg transits are automatically detected in the PIES record by locating parabolic fits within a sliding window, six early echos in width, that moves through the record. Once identified, it is assumed that
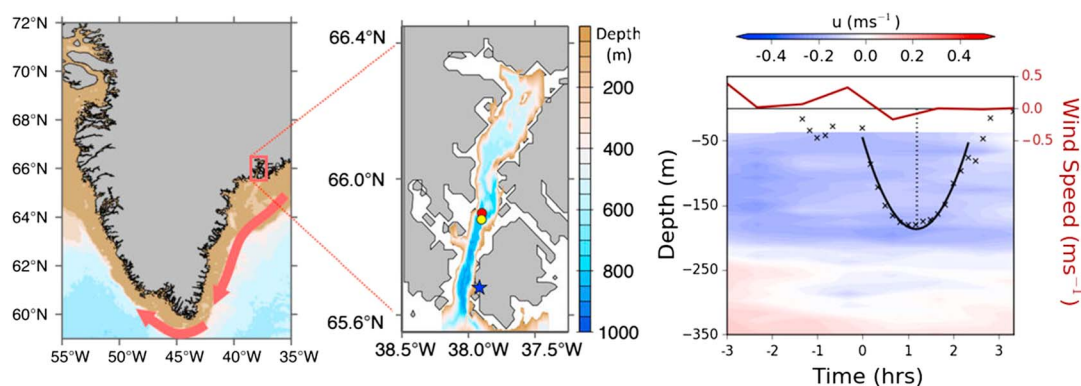
Figure 1. (left) Bathymetry and large-scale ocean circulation in southeast Greenland, with the red box marking Sermilik Fjord. (middle) Location of the ADCP (yellow circle), PIES (red circle), and weather station (blue star) in Sermilik Fjord. (right) Sample profile of an iceberg passing over the PIES visible in early echos recorded by the sensor (black crosses), with concurrent along-fjord ocean velocity data (shading) and along-fjord wind data (red line). The solid black line indicates the parabolic fit to the early echos (from which the iceberg speed is obtained), with time 0 defined as the start of the fit and the vertical dashed black line marking the minimum draft of the iceberg.

near the minimum of this parabola, all pings bounced off the same point on the passing iceberg. Thus, the parabola's curvature directly relates to the speed with which this point first approached, then receded from the sensor, and so may be used to calculate the iceberg's speed. A draft range may also be obtained, bounded by a minimum draft corresponding to an iceberg passing directly over the sensor, and a maximum draft corresponding to its passing the region ensonified by the PIES tangentially. Figure 1 (right) illustrates a typical iceberg transit in the PIES record, with the parabola fitted to it. Here the curvature of this fit gives an iceberg speed of 0.1 m s^{-1}.

3.2. Ocean Velocity and Wind Data

A 75 kHz acoustic Doppler current profiler (ADCP) was deployed in Sermilik Fjord from August 2011 to June 2012, as described in *Jackson et al.* [2014]. This sensor measured velocity in the water column between depths of 388 m and 40 m in 10 m bins at hourly intervals. We assume that icebergs moving past the PIES feel the same ocean velocity as that recorded by the ADCP. This is reasonable since the distance between the ADCP and the PIES (2 km) is small compared to the distance over which currents vary in the fjord and the lengthscales over which icebergs change velocity [*Jackson et al.*, 2014; *Sutherland et al.*, 2014].

Wind data were obtained at 10 min intervals during the study period from the Station Coast weather station [*Mernild and Hansen*, 2008; *Oltmanns et al.*, 2015] located 25 m above sea level at the fjord mouth (Figure 1), 24 km from the ADCP. Ocean current and wind data were rotated into the along-fjord direction (32° from north), with flows up fjord toward the calving face of Helheim glacier taken as positive.

3.3. Behavior of Icebergs in Sermilik Fjord

During summer, the PIES record was too noisy to identify parabolic transits, possibly due to increased biology or sediment in the water column producing many early reflections. From 26 February to 10 March 2012, land-fast sea ice was present [*Andres et al.*, 2015] and no transits were recorded. Excepting this 2 week period, 90 clean transits were recorded between November and June. The average iceberg speed was 0.09 m s^{-1}, with range 0.02 m s^{-1} to 0.24 m s^{-1}. The average minimum iceberg draft (obtained assuming the iceberg passed directly over the sensor) was 148 m, and the total draft range was 7 m to 490 m.

Iceberg speed was strongly correlated with ocean velocity vertically integrated over draft (Figure 2a), while there was negligible correlation between iceberg speed and along-fjord wind speed (Figure 2b), suggesting that it is predominantly ocean forcing that controls iceberg motion in the fjord. Iceberg draft was uncorrelated with iceberg speed, but note that the fastest icebergs had drafts of around 180 m (Figure 2c), the average depth of the interface between the deeper Atlantic water (AW) layer and upper polar water (PW) layer in Sermilik Fjord [*Jackson et al.*, 2014]. A plausible explanation is that shallower icebergs are more easily slowed by surface drag associated with sea ice and bergy bits and deeper icebergs experience a more greatly sheared ocean flow, enabling intermediate draft icebergs to travel the fastest.
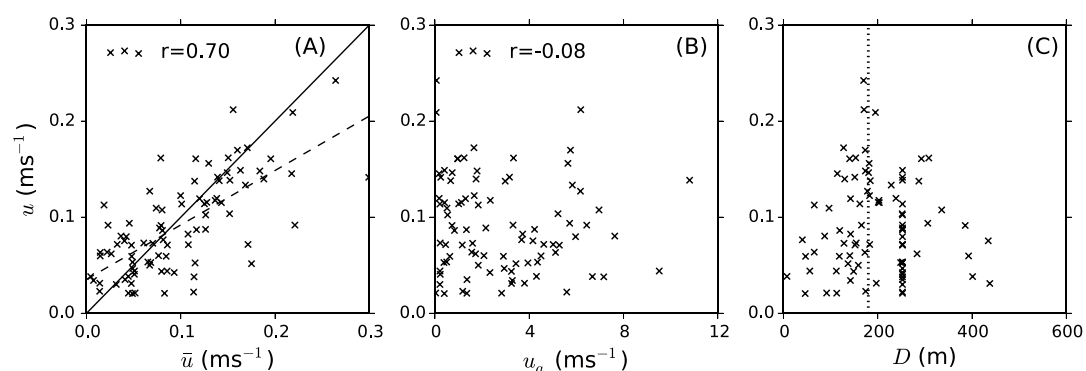
Figure 2. Dependence of observed iceberg speed u (from parabolic fit to PIES record) on (a) integrated ocean velocity over the iceberg draft $\bar{u}$ (dashed line indicates best fit), (b) along-fjord wind speed u_a during its passage over the sensor, and (c) iceberg draft as deduced from the model in section 4. The vertical dashed line marks the average depth (180 m [*Jackson et al.*, 2014]) of the interface between the upper layer of Polar water and the deeper layer of Atlantic water in the fjord.

4. Model

In section 3.1, we explained how iceberg speeds and draft ranges could be deduced from the PIES early echo record. To determine relative ocean velocity profiles felt by iceberg keels in Sermilik Fjord, we must also provide a direction of motion and a single value of the draft for the icebergs. To do this, we used a one-dimensional steady state simplification of the canonical model of iceberg motion (equation (1)) to supplement the data, and neglected wave forces, pressure gradient forces, and stresses due to the presence of sea ice. The validity of these simplifications and the assumption that icebergs may be modeled as cuboids and are in steady state with their forcings are examined in the supporting information.

With the above assumptions, the momentum equation (1) becomes

$$\tau_a + \tau_o = 0, \tag{3}$$

so wind and ocean stresses on the iceberg are balanced and the iceberg moves at a constant speed. Stress terms τ_a and τ_o are calculated by integrating air and ocean forces over the iceberg freeboard F and draft D (where $D/(F + D) = 0.8$), respectively. For a cuboid iceberg of draft D and velocity u, the stress terms have the form

$$\tau_a = \rho_a C_a |u_a - u|(u_a - u)F, \tag{4}$$

$$\tau_o = \rho_o C_o \int_{-D}^{0} |u_o(z) - u|(u_o(z) - u) \, \mathrm{d}z. \tag{5}$$

The subscripts a and o indicate atmospheric and oceanic properties, respectively, with ρ the fluid's density and C the fluid's dimensionless drag coefficient.

Following a sensitivity analysis (see supporting information), we tuned the one-dimensional model with the standard ocean and atmospheric drag coefficients of *Bigg et al.* [1997], with values of 0.9 and 1.3, respectively. To obtain the approximate steady state forcing on the iceberg, we averaged ocean currents and winds from 6 h prior to the iceberg's transit over the PIES, to when the iceberg left the sensor's field of view.

For each iceberg record, concurrent wind and ocean velocity data were extracted and averaged over the requisite time period. There is no ocean velocity data from the ADCP record over the top 40 m of the water column, so the velocity gradient in the three 10 m bins closest to the surface was extrapolated to obtain the velocity in this layer (as discussed in the supporting information). Given the ocean and air velocities associated with the iceberg transit, an optimization algorithm was run to minimize the cost function $|\tau_a + \tau_o|$ for varying values of iceberg velocity u. This was conducted for three values of iceberg draft in the observed draft range: the minimum possible draft, the maximum possible draft, and the mean of the minimum and maximum drafts. The fitted velocity magnitude was then compared to the observed speed, and the iceberg draft was taken to be that which gave the best fit to this observed speed. Note that whereas the minimum and average drafts vary continuously, 252 m is the upper bound on iceberg draft of any shallow icebergs [*Andres et al.*, 2015], explaining the larger number of icebergs with this draft in Figure 2c.
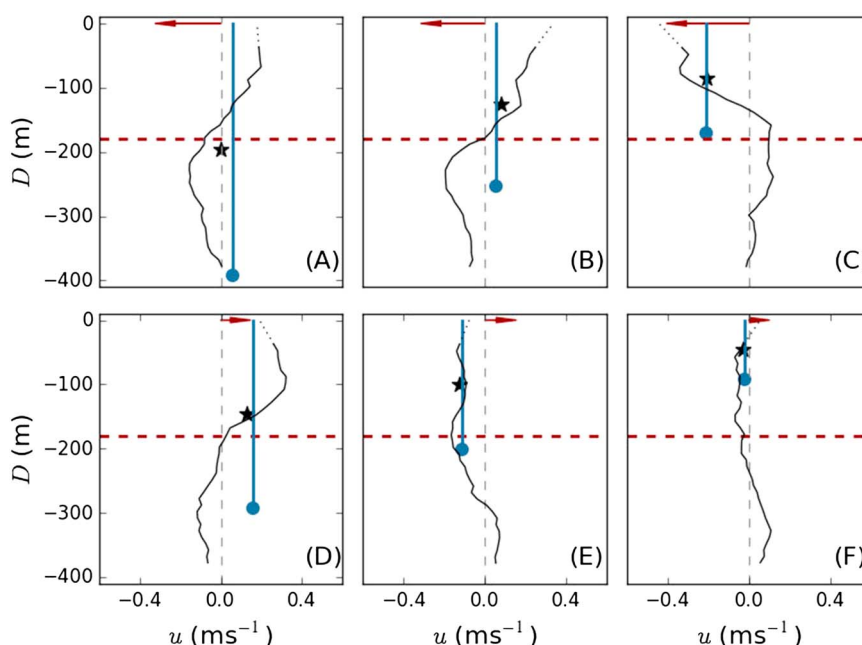
Figure 3. Example profiles of along-fjord velocities felt by icebergs for six transit events (a–f) from the record. In each panel, the iceberg draft and velocity (from model-supplemented observations) are illustrated by the vertical blue line. The profile in black is the average ocean velocity during the passage of the iceberg over the sensor and the 6 h period prior to its passage, with the extrapolated velocity in the top 40 m of the water column marked by the dashed extension of this profile and the vertical average velocity over the iceberg draft marked by the black star. The wind speed and direction during the event are indicated by the red arrow (scaled by factor 5). The horizontal dashed lines indicate the average interface depth between the upper PW and deeper AW layers in the fjord [*Jackson et al.*, 2014].

The simplified model successfully reproduced observed iceberg speeds, with a correlation coefficient of 0.8 between observed and modeled speeds. This agreement gave confidence that the model simplifications were reasonable for Sermilik Fjord and allowed us to proceed based on the velocity signs and drafts produced by the model.

5. Results

5.1. Typical Iceberg Transit Profiles

By combining our observational record of iceberg speeds and draft ranges with modeled iceberg velocity signs and precise drafts, we could fully describe the icebergs' motion in the along-fjord direction during their transit over the PIES. For each iceberg passage event, we compared the iceberg's velocity and draft to the concurrent ADCP record of ocean currents to obtain the relative velocity profile felt by the iceberg.

A selection of typical velocity profiles felt by icebergs passing over the sensor is shown in Figure 3. It can be seen that while some icebergs (e.g., Figures 3e and 3f) feel a homogeneous ocean velocity and hence experience little relative velocity with respect to the ocean, 80% of icebergs experience a range greater than $0.2 \, \mathrm{m \, s^{-1}}$ in ocean velocity over their draft and move with approximately the average of this profile. This average differs substantially from the surface velocity, whether taken as the velocity in the shallowest ADCP bin or the linear extrapolation of the ADCP measurements to the surface layer. The largest velocity gradient is often associated with the transition from the PW to the AW layer in the fjord, and as such icebergs with drafts deeper than the average depth of this interface (180 m) are particularly prone to shear.

Note that the velocity profiles depicted are time averages (from 6 h prior to the iceberg's transit over the sensor until the time the iceberg leaves the field of view of the PIES), and instantaneous ocean velocity profiles can show even greater shear. Further, even greater relative velocity magnitudes might be anticipated for grounded icebergs that no longer move with the vertically integrated ocean velocity.

5.2. Error Incurred From Neglecting Shear

Given the prevalence of vertical shear in the ocean velocity profiles from the observational record, it is of interest to iceberg modeling to quantify error incurred by using surface ocean velocities in the parameterizations
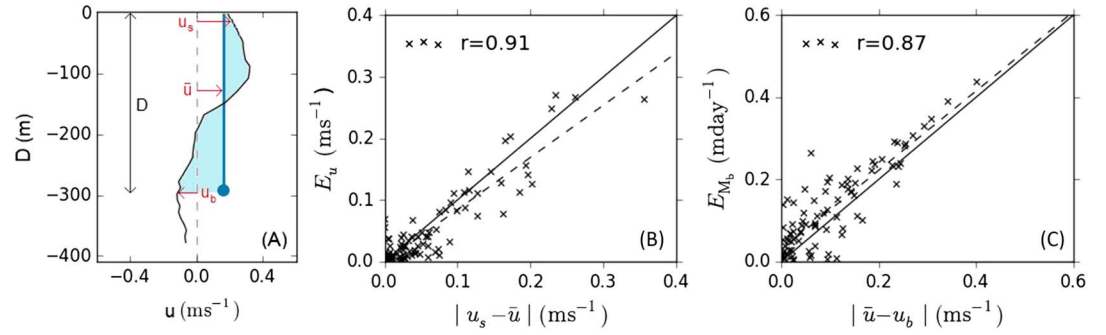
Figure 4. Dependence of error in iceberg velocity and melt on ocean shear. (a) Definition of surface speed u_s, average speed $\bar{u}$, and basal speed u_b for an iceberg of draft D. (b) Error in iceberg speed due to applying the surface velocity as opposed to the depth-varying velocity in the model, as a function of the difference between the iceberg and the surface current $|u_s - \bar{u}|$. (c) Error in iceberg basal melt rate due to using the surface velocity rather than the basal velocity, as a function of the difference between the iceberg and the basal current $|\bar{u} - u_b|$. The best fits in Figures 4b and 4c are marked with dashed lines and the corresponding correlation coefficients labeled.

of iceberg motion and melt. This can be calculated, in the case of a one-dimensional force balance model, only in the absence of wind stress. Using equation (5), the simplified model of iceberg motion becomes

$$\tau_o \equiv \rho_o C_o \int_{-D}^{0} |u_o(z) - u|(u_o(z) - u)\, dz = 0. \tag{6}$$

The absolute value within the integral makes this analytically intractable when $u_o - u$ changes sign over the iceberg draft, but proceeding by assuming $u_o - u$ has a constant sign, and this is minimized as a function of u when $u = \bar{u}$ for $\bar{u} \equiv \frac{1}{D} \int_{-D}^{0} u_o(z)\, dz$. In contrast, if just the surface ocean velocity is considered, the equation of motion is

$$\tau_o \equiv \rho_o C_o D |u_s - u|(u_s - u) = 0, \tag{7}$$

and $u = u_s$ (where $u_s \equiv u_o|_{z=0}$). The error in iceberg speed incurred from neglecting the ocean shear is thus

$$E_u = |u_s - \bar{u}|. \tag{8}$$

We run our model twice, once calculating iceberg velocity using the full depth-varying ocean currents and once using only the surface ocean currents. Differencing the resulting speeds gives the E_u, shown as a function of the theoretical error $|u_s - \bar{u}|$ in Figure 4b. Divergences from theoretical error may be attributed to the influence of winds in the model, not accounted for in the calculation above.

If in equation (2) for iceberg basal melt we assume that the relevant ocean velocity is the surface velocity and if the iceberg equations of motion are simplified as in equation (7), this parameterization unphysically gives that the iceberg experiences no basal melt. If instead, as observed, the iceberg moves with approximately a speed $\bar{u}$ and we consider the basal velocity $u_b = u_o|_{z=-D}$ as the relevant ocean velocity in equation (2), the basal melt rate is given by

$$M_b = 0.58 \frac{T_o - T}{L^{0.2}} |\bar{u} - u_b|^{0.8}. \tag{9}$$

It follows that $E_{M_B} \sim |\bar{u} - u_b|^{0.8}$ and the largest melt rate error occurs when the basal velocity diverges significantly from the mean velocity.

The model-calculated E_{M_b} is obtained by differencing the basal melt rate computed using the surface ocean velocity and assuming that the iceberg feels the surface currents only in its equation of motion and the basal melt rate computed using the ocean velocity at the bottom of the iceberg and allowing the iceberg to feel the ocean currents over its entire draft. This is compared to the difference between the average and basal velocities $|\bar{u} - u_b|$ in Figure 4c. There is a broader spread in E_{M_b} than in E_u due to the dependence of E_{M_b} on iceberg length L through the factor $1/L^{0.2}$. In the model, L is approximated as $2D$ (based on the characteristic aspect ratio of icebergs in Greenlandic fjords [*Enderlin et al.*, 2016]). In calculating melt rates, we assume a constant ocean temperature of 2°C, lying between that of the warmer AW and that of the cooler PW in Sermilik Fjord [*Jackson et al.*, 2014]. Note that there are two sources of error in the parameterized basal melt rate: that incurred from moving the iceberg with just the surface currents, resulting in an incorrect iceberg speed, and that from melting the iceberg with the surface relative velocity as opposed to the basal relative velocity.

5.3. Discussion

The mean iceberg speed in our observational record was around 0.1 m s^{-1}, and the mean difference $|\bar{u} - u_s|$ was 0.06 m s^{-1}, indicating an average speed error of 60% from using, in the momentum equation, surface ocean currents as opposed to ocean currents over the full depth of the iceberg. This error increased to 0.26 m s^{-1} (260% of mean iceberg speed) for the maximum difference of 0.36 m s^{-1}.

For the parameterization of iceberg melt in climate models, ocean velocity enters through the bottom melt term M_b, which (using the standard parameterization) may typically be up to 1 m d^{-1} [*Bigg*, 2016] in the open ocean. For icebergs in Sermilik Fjord, *Enderlin and Hamilton* [2014] estimate a total submarine melt rate of 0.39 m d^{-1}. Based on an ocean temperature of 2°C, the mean basal melt rate in our study when using u_b for ocean velocity was 0.17 m d^{-1}, varying between 0.01 m d^{-1} and 0.49 m d^{-1}. The mean $E_{M_b} = 0.12 \text{ m d}^{-1}$ represents an error of 71% relative to this mean melt rate and increases to a 259% error for the maximum $E_{M_b} = 0.44 \text{ m d}^{-1}$. The total iceberg melt rate is the sum of side melt and wave erosion in addition to bottom melt. Consequently, the error in the bottom melt term will affect more those icebergs and environments in which bottom melt dominates, namely, tabular icebergs in relatively warm waters.

While there has been some recent modeling effort to include in icebergs' equation of motion the ocean currents over the range of their draft [*Kubat et al.*, 2005, 2007; *Hill and Condron*, 2014; *Marsh et al.*, 2015; *Merino et al.*, 2016], we are unaware of any effort to account for the effect of shear on iceberg melt. Here we have limited our discussion to the effect of a sheared flow on the bottom melt of icebergs. However, it is anticipated that a nonzero relative velocity will also influence the side melt of icebergs, despite this term not being present in the current parameterization. This would further add to the error incurred by using surface ocean velocities to estimate iceberg melt. Further work is needed to incorporate a relative velocity into the parameterization of the side melt of icebergs. A study investigating this process using laboratory experiments will be the focus of a future contribution.

6. Conclusions

In this work we have discussed an extensive and unique iceberg and ocean velocity record in Sermilik Fjord, Greenland. Iceberg motion in the fjord was shown to be dominated by the vertical average of the ocean currents over the draft of the iceberg. Perhaps as a consequence, icebergs with drafts close to the interface between the upper PW and lower AW layers in the fjord had the fastest observed speeds, being least affected by the shear between the ocean layers or surface drag. It was found that strongly sheared flows significantly impact iceberg velocity and basal melting, with average errors of 60% in modeled speed and 71% in modeled basal melt if this shear is neglected. These large error values highlight the importance of including depth varying ocean velocities in parameterizations of iceberg motion and melt.

The evidence presented here that icebergs are subject to strongly sheared flows over their draft emphasizes the need for a new parameterization of the side melt of icebergs that takes into account the effect of ambient velocity. The effect of ocean current shear on icebergs may be particularly important when computing the heat and salinity budget of Greenlandic fjords, due to their strongly sheared nature and the fact iceberg melt inside these fjords is a major contributor to freshwater export [*Jackson and Straneo*, 2016]. Although currents around Antarctica are typically less sheared than those in Greenlandic fjords, dimensions of Antarctic icebergs can be an order-of-magnitude larger than those observed around Greenland [*Savage*, 2001]. The large drafts of giant icebergs calving into the Southern Ocean means that there may still be significant variation in ocean velocity over the draft of the iceberg. In such cases, a consideration of the shear felt by the iceberg may also improve the modeling of icebergs.

References

Andres, M., A. Silvano, F. Straneo, and D. R. Watts (2015), Icebergs and sea ice detected with inverted echo sounders, *J. Atmos. Oceanic Technol.*, *32*(5), 1042–1057.

Bamber, J. L., and W. P. Aspinall (2013), An expert judgement assessment of future sea level rise from the ice sheets, *Nat. Clim. Change*, *3*(4), 424–427.

Bigg, G. R. (2016), The physics of icebergs, in *Icebergs: Their Science and Links to Global Change*, chap. 3, pp. 52–81, Cambridge Univ. Press, Cambridge, U. K.

Bigg, G. R., M. R. Wadley, D. P. Stevens, and J. A. Johnson (1997), Modelling the dynamics and thermodynamics of icebergs, *Cold Reg. Sci. Technol.*, *26*(2), 113–135.

Depoorter, M. A., J. L. Bamber, J. A. Griggs, J. T. M. Lenaerts, S. R. M. Ligtenberg, M. R. van den Broeke, and G. Moholdt (2013), Calving fluxes and basal melt rates of Antarctic ice shelves, *Nature*, *502*(7469), 89–92.

Duprat, L. P. A. M., G. R. Bigg, and D. J. Wilton (2016), Enhanced Southern Ocean marine productivity due to fertilization by giant icebergs, *Nat. Geosci.*, *9*(1), 219–221.

El-Tahan, M., S. Venkatesh, and H. El-Tahan (1987), Validation and quantitative assessment of the deterioration mechanisms of Arctic icebergs, *J. Offshore Mech. Arct. Eng.*, *109*(1), 102–108.

Enderlin, E., and I. Howat (2014), An improved mass budget for the Greenland ice sheet, *Geophys. Res. Lett.*, *41*, 866–872, doi:10.1002/2013GL059010.

Enderlin, E. M., and G. S. Hamilton (2014), Estimates of iceberg submarine melting from high-resolution digital elevation models: Application to Sermilik Fjord, east Greenland, *J. Glaciol.*, *60*(224), 1111–1116.

Enderlin, E. M., G. S. Hamilton, F. Straneo, and D. A. Sutherland (2016), Iceberg meltwater fluxes dominate the freshwater budget in Greenland's iceberg-congested glacial fjords, *Geophys. Res. Lett.*, *43*, 11,287–11,294, doi:10.1002/2016GL070718.

Gladstone, R. M., G. R. Bigg, and K. W. Nicholls (2001), Iceberg trajectory modeling and meltwater injection in the Southern Ocean, *J. Geophys. Res.*, *106*(C9), 19,903–19,915.

Hill, J. C., and A. Condron (2014), Subtropical iceberg scours and meltwater routing in the deglacial western North Atlantic, *Nat. Geosci.*, *7*(11), 806–810.

Jackson, R. H., and F. Straneo (2016), Heat, salt and freshwater budgets for a glacial fjord in Greenland, *J. Phys. Oceanogr.*, *46*, 2735–2768.

Jackson, R. H., F. Straneo, and D. A. Sutherland (2014), Externally forced fluctuations in ocean temperature at Greenland glaciers in non-summer months, *Nat. Geosci.*, *7*(7), 503–508.

Kubat, I., M. Sayed, S. B. Savage, and T. Carrieres (2005), An operational model of iceberg drift, *Int. J. Offshore Polar Eng.*, *15*(2), 1–7.

Kubat, I., M. Sayed, S. Savage, T. Carrieres, and G. Crocker (2007), An operational iceberg deterioration model. paper presented at 16th International Offshore and Polar Engineering Conference, pp. 652–657.

Marsh, R., et al. (2015), NEMO–ICB (v1.0): Interactive icebergs in the NEMO ocean model globally configured at eddy-permitting resolution, *Geosci. Model Dev.*, *8*(5), 1547–1562.

Martin, T., and A. Adcroft (2010), Parameterizing the fresh-water flux from land ice to ocean with interactive icebergs in a coupled climate model, *Ocean Modell.*, *34*(3–4), 111–124.

Merino, I., J. Le Sommer, G. Durand, N. C. Jourdain, G. Madec, P. Mathiot, and J. Tournadre (2016), Antarctic icebergs melt over the Southern Ocean: Climatology and impact on sea-ice, *Ocean Modell.*, *104*, 99–110.

Mernild, S., and B. Hansen (2008), Climatic conditions at the Mittivakkat Glacier catchment (1994–2006), Ammassalik Island, SE Greenland, and in a 109-year perspective (1898–2006), *Geogr. Tidsskr.-Danish J. Geogr.*, *1*(1), 51–72.

Mountain, D. G. (1980), On predicting iceberg drift, *Cold Reg. Sci. Technol.*, *1*(3–4), 273–282.

Neshyba, S., and E. G. Josberger (1980), On the estimation of Antarctic iceberg melt rate, *J. Phys. Oceanogr.*, *10*(10), 1681–1685.

Oltmanns, M., F. Straneo, H. Seo, and G. W. K. Moore (2015), The role of wave dynamics and small-scale topography for downslope wind events in southeast Greenland, *J. Atmos. Sci.*, *72*(7), 2786–2805.

Rignot, E., J. E. Box, E. Burgess, and E. Hanna (2008), Mass balance of the Greenland ice sheet from 1958 to 2007, *Geophys. Res. Lett.*, *35*, L20502, doi:10.1029/2008GL035417.

Rignot, E., I. Velicogna, M. R. Van den Broeke, A. Monaghan, and J. T. M. Lenaerts (2011), Acceleration of the contribution of the Greenland and Antarctic ice sheets to sea level rise, *Geophys. Res. Lett.*, *38*, L05503, doi:10.1029/2011GL046583.

Savage, S. B. (2001), Aspects of iceberg deterioration and drift, *Geomorphol. Fluid Mech.*, *582*, 279–318.

Smith, S. D. (1993), Hindcasting iceberg drift using current profiles and winds, *Cold Reg. Sci. Technol.*, *22*(1), 33–45.

Srokosz, M., M. Baringer, H. Bryden, S. Cunningham, T. Delworth, S. Lozier, J. Marotzke, and R. Sutton (2012), Past, present, and future changes in the Atlantic Meridional Overturning Circulation, *Bull. Am. Meteorol. Soc.*, *93*(11), 1663–1676.

Sutherland, D. A., G. Roth, G. S. Hamilton, S. Mernild, L. A. Stearns, and F. Straneo (2014), Quantifying flow regimes in a Greenland glacial fjord using iceberg drifters, *Geophys. Res. Lett.*, *41*, 8411–8420, doi:10.1002/2014GL062256.

Weeks, W. F., and W. J. Campbell (1973), Icebergs as a fresh-water source: An appraisal, *J. Glaciol.*, *12*(65), 207–233.

Zickfeld, K., A. Levermann, M. G. Morgan, T. Kuhlbrodt, S. Rahmstorf, and D. W. Keith (2007), Expert judgements on the response of the Atlantic Meridional Overturning Circulation to climate change, *Clim. Change*, *82*(3–4), 235–265.